Study of the hidden charm $D\bar{D}^*$ interactions in chiral effective field theory

Hao Xu *

Institute of Theoretical Physics, College of Physics and Electronic Engineering,
Northwest Normal University, Lanzhou 730070, China
and Lanzhou Center for Theoretical Physics, Lanzhou University, Lanzhou 730000, China

We study the chiral interactions of the hidden charm $D\bar{D}^*$ system within chiral effective field theory. Chiral Lagrangians are constructed by incorporating the chiral symmetry, heavy quark symmetry, as well as proper charge conjugation properties of the heavy mesons. The interacting potentials of the S-wave $D\bar{D}^*$ system are calculated up to the second chiral order at a one-loop level, where complete two-pion exchange interactions are included. We further investigate the behaviors of the potentials in coordinate space, and their bound state properties. Our studies indicate that there exists an interacting strength ordering among considered four channels: str.$[0^+(1^{++})] >$ str.$[0^-(1^{+-})] >$ str.$[1^+(1^{+-})] >$ str.$[1^-(1^{++})]$, where str. stands for the strength of the $D\bar{D}^*$ interaction. Moreover, we find that $X(3872)$ can be treated as a good candidate of the $0^+(1^{++})$ molecular state. $D\bar{D}^*$ also tends to form $0^-(1^{+-})$ and $1^+(1^{+-})$ molecular states, and we expect future experiments to search for the predicted multiple structures around the $D\bar{D}^*$ mass region.

I. INTRODUCTION

In past two decades, abundant exotic hadrons have been discovered by upgraded τ-charm and b factories, such as BESIII, LHCb, Belle, *BABAR*, etc. Till now, various forms of exotic quark matters arise in hadron spectroscopy: pentaquarks (P_c and P_{cs} states), fully charmed tetraquark candidates [recently discovered $X(6900)$], hidden charm tetraquark candidates (some XYZ states), etc. For example, $X(6900)$ was discovered by LHCb recently [1], which appears to be a nontrivial structure in the di-J/ψ invariant mass spectrum. Subsequently, the LHCb Collaboration also reported two structures $X_0(2900)$ and $X_1(2900)$ in the $B^+ \to D^+D^-K^+$ decay [2], which are supposed to have four different flavors: $\bar{c}\bar{s}ud$. Until very recently, LHCb observed a doubly charmed structure T_{cc} [3] that is extremely close to the D^0D^{*+} threshold (the mass difference is $-273 \pm 61 \pm 5^{+11}_{-14}$ keV). T_{cc} has a minimal $cc\bar{u}\bar{d}$ content. Therefore, it may still be an ongoing progress that other forms of multiquark structures are prepared to be uncovered. The rapidly growing numbers of exotic hadrons urgently demand us to extend our knowledge about nonperturbative QCD.

Although the studies of the exotic hadrons on experimental side are in advance, their natures and inner structures are still unclear. Theorists try to understand them with all kinds of methods and models (see Refs. [4–9] for reviews of theoretical as well as experimental status).

For example, people still cannot truly understand the nature of the first observed XYZ state, $X(3872)$ [also known as $\chi_{c1}(3872)$]. $X(3872)$ was discovered by the Belle collaboration in $B^{+-} \to K^{+-}\pi^+\pi^-J/\psi$ [10]. It may be regarded as a charmonium $\chi'_{c1}(2P)$, but its mass would be much lower than a quark model estimate (e.g., the Godfrey-Isgur (GI) model calculation in Ref. [11]). Furthermore, it also has a large decay ratio in the isospin violation process $X(3872) \to J/\psi\rho$. It is noteworthy that $X(3872)$ is almost located at the $D^0\bar{D}^{*0}$ threshold, so it is believed that the interaction between $D\bar{D}^*$ is responsible for the formation of $X(3872)$.

Besides $X(3872)$, there are many other XYZ states that may be strongly related to open-charm thresholds. The charged charmoniumlike state $Z_c(3900)$ was observed in the process $e^+e^- \to J/\psi\pi^+\pi^-$ [12,13]. With the mass slightly above the $D\bar{D}^*$ threshold, it may originate from the $D\bar{D}^*$ interaction. Other states such as $Z_c(4020)$ [14], $Y(3940)$ [15], and $Y(4140)$ [16] are close to respective $D^*\bar{D}^*$ and $D^*_s\bar{D}^*_s$ thresholds too. There also exist some higher XYZ states that are close to excited open-charm thresholds: $Z_c^+(4430)$ [17] with $D^*\bar{D}_1^{(\prime)}$, recently discovered $Y(4626)$ [18] [and $Y(4620)$ [19]] with $D^*_s\bar{D}_{s1}$, and etc.

*xuh2020@nwnu.edu.cn

034013-1

Taking into account the interactions of these open-charm meson pairs, people have tried to explain these XYZ states with various phenomenological models, such as the one-boson-exchange model [4,20].

Therefore, for understanding the XYZ states mentioned above, it is crucial to elaborately investigate corresponding charmed- anticharmed meson interactions within a proper theoretical framework. Chiral effective field theory (ChEFT) is the powerful formalism that just satisfies the need. Other than phenomenological models, in ChEFT, the interactions between hadrons are strictly and systematically calculated up to a given order, while all contributions such as the multipion exchange are contained completely. Especially, in our case (i.e., heavy-heavy system), Weinberg's scheme is adopted [21,22], which has been widely used to investigate the nucleon-nucleon interaction [23–44] (see Refs. [45–49] for reviews). So it is natural to extend the framework to the sector of the heavy hadron interactions.

The authors in Refs. [50,51] have already made attempts to study heavy meson systems with heavy meson chiral effective field theory (HMChEFT). The authors in Ref. [50] calculated the potentials of the doubly bottomed system $\bar{B}\bar{B}$ with contact and two pion exchange mechanisms under HMChEFT. Later, the authors in Ref. [51] developed corresponding techniques and investigated the doubly charmed system DD^*, then further utilized the Schrödinger equation to search for bound state solutions. Following the same procedures, the authors in Refs. [52–58] studied the interactions of other heavy hadron systems.

With the experience in the studies of the doubly heavy-flavored systems mentioned above, it is natural to extend them to the heavy-antiheavy flavored systems, which will be directly linked to the charmoniumlike states talked before. Note that this extension is not straightforward; for example, the interactions of the heavy-antiheavy flavored systems should be constructed by properly considering the charge conjugation properties of the fields in the heavy quark limit.

In this work, choosing the charmed-anticharmed system $D\bar{D}^*$ as an example, we will try to study the $D\bar{D}^*$ interactions up to the second chiral order $O(\epsilon^2)$ at then one-loop level using Weinberg's scheme. The contribution carrying contact interactions, the contributions of one-pion exchange (OPE) and two-pion exchange (TPE) will be included completely. As mentioned above, different from calculated doubly heavy-flavored systems before [50,51], additional symmetries (the charge conjugation symmetry) as well as proper charge conjugation states should be concerned when constructing the $D\bar{D}^*$ inter-actions and $D\bar{D}^*$ scattering amplitudes.

Following the strategy in Ref. [51], we will iterate the obtained $D\bar{D}^*$ potentials into the Schrödinger equation, to see whether the $D\bar{D}^*$ interactions are strong enough to form bound states. It is noteworthy that under the one-boson-exchange model, the authors in Refs. [20,59–62] also

studied the $D\bar{D}^*$ system, they considered one boson (π, σ, ρ, ω, etc.) exchange mechanism. They found that $D\bar{D}^*$ in the $J^{PC} = 1^{++}$, $I = 0$ channel [J^{PC} of $X(3872)$], as well as some other channels, are strong enough to form bound states. Therefore, results and conclusions presented in this work may be a comparison to theirs. In addition, the authors in Ref. [63] also studied the $D\bar{D}^*$ system and $X(3872)$ in the one-boson-exchange model. Also, the authors in Ref. [64] studied the $D\bar{D}^*$ hadronic molecules in effective field theory early in 2006. Possible $D\bar{D}^*$ molecular states also have been studied extensively in various methods [65–84].

This paper is organized as follows. In Sec. II we describe the concerned $D\bar{D}^*$ Lagrangians by considering the chiral symmetry and heavy quark symmetry, as well as by properly taking into account the charge conjugation proper-ties of the heavy mesons. In Sec. III we calculate the potentials of the $D\bar{D}^*$ system up to the second chiral order $O(\epsilon^2)$ at one-loop level using Weinberg's scheme. In Sec. IV, after solving the Schrödinger equation with calculated $D\bar{D}^*$ potentials, we investigate the bound state properties in the considered four channels. Then we discuss the behaviors of the potentials in coordinate space to further understand the $D\bar{D}^*$ interactions and the mechanisms of the bound state formations. Later we discuss the obtained molecular states and their discovery potentials in detail. The last section is the summary.

II. CHIRAL LAGRANGIANS OF THE $D\bar{D}^*$ SYSTEM IN HMChEFT

Like Refs. [50,51], we adopt HMChEFT, and derive the Lagrangians and effective potentials in a strict power-counting scheme. In this framework, the amplitudes or potentials are arranged according to the chiral order $\epsilon = p/\Lambda_\chi$ (p stands for the momentum of a pion, or a residual momentum of a heavy meson, or the $D - D^*$ mass splitting). In this work the flavor $SU(2)$ symmetry is considered.

We first show the Lagrangians of the concerned $D\bar{D}^*$ system at leading order. First, the $DD^*\pi$ Lagrangian at $O(\epsilon^1)$ is needed [85–87]:

$$\mathcal{L}_{H\phi}^{(1)} = -\langle (iv \cdot \partial H)\bar{H}\rangle + \langle Hv \cdot \Gamma \bar{H}\rangle + g\langle H\slashed{u}\gamma_5\bar{H}\rangle - \frac{1}{8}\delta\langle H\sigma^{\mu\nu}\bar{H}\sigma_{\mu\nu}\rangle, \tag{1}$$

where the H field describing the (D, D^*) doublet is

$$H = \frac{1 + \slashed{v}}{2}(P_\mu^*\gamma^\mu + iP\gamma_5),$$

$$\bar{H} = \gamma^0 H^\dagger \gamma^0 = (P_\mu^{*\dagger}\gamma^\mu + iP^\dagger\gamma_5)\frac{1 + \slashed{v}}{2},$$

$$P = (D^0, D^+), \qquad P_\mu^* = (D^{*0}, D^{*+})_\mu. \tag{2}$$

$v = (1, 0, 0, 0)$ stands for the four velocity of the H field. The axial vector field u and chiral connection Γ are expressed as

$$\Gamma_\mu = \frac{i}{2}[\xi^\dagger, \partial_\mu \xi], \qquad u_\mu = \frac{i}{2}\{\xi^\dagger, \partial_\mu \xi\}, \qquad (3)$$

where $\xi = \exp(i\phi/2f)$, f is the bare pion decay constant, and

$$\phi = \sqrt{2}\begin{pmatrix} \frac{\pi^0}{\sqrt{2}} & \pi^+ \\ \pi^- & -\frac{\pi^0}{\sqrt{2}} \end{pmatrix}. \qquad (4)$$

For studying the $D\bar{D}^*$ system under HMChEFT, we also need to describe the interaction between an anticharmed meson and a pion. Applying charge conjugation transformation to Eq. (1), the Lagrangian of the interacting part is given by

$$\mathcal{L}_{H_c\phi}^{(1)} = -\langle \bar{H}_c v \cdot \Gamma H_c \rangle + g\langle \bar{H}_c \slashed{u} \gamma_5 H_c \rangle, \qquad (5)$$

where $g = 0.59$. In the above, H_c field represents the anticharmed meson doublet $(\bar{D}, \bar{D}^*)$ in the heavy quark limit, and the subscript c stands for charge conjugation.

Note that H_c is defined as charge conjugation of H in Eq. (1):

$$H_c = (P^*_{c\mu}\gamma^\mu + iP_c\gamma_5)\frac{1 - \slashed{v}}{2},$$

$$\bar{H}_c = \gamma^0 H_c^\dagger \gamma^0 = \frac{1 - \slashed{v}}{2}(P^{*\dagger}_{c\mu}\gamma^\mu + iP_c^\dagger \gamma_5),$$

$$P_c = (\bar{D}^0, D^-), \qquad P^*_{c\mu} = (\bar{D}^{*0}, D^{*-})_\mu. \qquad (6)$$

Then, the contact Lagrangian at $O(\epsilon^0)$ is needed for $O(\epsilon^0)$ and $O(\epsilon^2)$ amplitudes, which can be constructed as

$$\begin{aligned} \mathcal{L}_{2H2H_c}^{(0)} = &\, D_a \text{Tr}[H\gamma_\mu \bar{H}]\text{Tr}[\bar{H}_c\gamma^\mu H_c] \\ &+ D_b \text{Tr}[H\gamma_\mu\gamma_5 \bar{H}]\text{Tr}[\bar{H}_c\gamma^\mu\gamma_5 H_c] \\ &+ E_a \text{Tr}[H\gamma_\mu\tau^a \bar{H}]\text{Tr}[\bar{H}_c\gamma^\mu\tau_a H_c] \\ &+ E_b \text{Tr}[H\gamma_\mu\gamma_5\tau^a \bar{H}]\text{Tr}[\bar{H}_c\gamma^\mu\gamma_5\tau_a H_c], \quad (7) \end{aligned}$$

where D_a, D_b, E_a, E_b are four independent low energy constants (LECs).

For the loop diagrams in the potentials (or the amplitudes) at order $O(\epsilon^2)$, we also need $O(\epsilon^2)$ contact Lagrangians to cancel their divergences:

$$\begin{aligned} \mathcal{L}_{2H2H_c}^{(2,h)} = &\, D_a^h \text{Tr}[H\gamma_\mu \bar{H}]\text{Tr}[\bar{H}_c\gamma^\mu H_c]\text{Tr}(\chi_+) + D_b^h \text{Tr}[H\gamma_\mu\gamma_5 \bar{H}]\text{Tr}[\bar{H}_c\gamma^\mu\gamma_5 H_c]\text{Tr}(\chi_+) \\ &+ E_a^h \text{Tr}[H\gamma_\mu\tau^a \bar{H}]\text{Tr}[\bar{H}_c\gamma^\mu\tau_a H_c]\text{Tr}(\chi_+) + E_b^h \text{Tr}[H\gamma_\mu\gamma_5\tau^a \bar{H}]\text{Tr}[\bar{H}_c\gamma^\mu\gamma_5\tau_a H_c]\text{Tr}(\chi_+), \quad (8) \end{aligned}$$

$$\begin{aligned} \mathcal{L}_{2H2H_c}^{(2,v)} = &\, D_{a1}^v(\text{Tr}[(v \cdot DH)\gamma_\mu(v \cdot D\bar{H})]\text{Tr}[\bar{H}_c\gamma^\mu H_c] + \text{C.c.}) + D_{a2}^v(\text{Tr}[(v \cdot DH)\gamma_\mu \bar{H}]\text{Tr}[(v \cdot D\bar{H}_c)\gamma^\mu H_c] + \text{C.c.}) \\ &+ D_{a3}^v(\text{Tr}[(v \cdot DH)\gamma_\mu \bar{H}]\text{Tr}[\bar{H}_c\gamma^\mu(v \cdot DH_c)] + \text{H.c.}) + D_{a4}^v([\text{Tr}[((v \cdot D)^2 H)\gamma_\mu \bar{H}]\text{Tr}[\bar{H}_c\gamma^\mu H_c] + \text{H.c.}] + \text{C.c.}) \\ &+ D_{b1}^v(\text{Tr}[(v \cdot DH)\gamma_\mu\gamma_5(v \cdot D\bar{H})]\text{Tr}[\bar{H}_c\gamma^\mu\gamma_5 H_c] + \text{C.c.}) + \ldots \\ &+ E_{a1}^v(\text{Tr}[(v \cdot DH)\gamma_\mu\tau^a(v \cdot D\bar{H})]\text{Tr}[\bar{H}_c\gamma^\mu\tau_a H_c] + \text{C.c.}) + \ldots \\ &+ E_{b1}^v(\text{Tr}[(v \cdot DH)\gamma_\mu\gamma_5\tau^a(v \cdot D\bar{H})]\text{Tr}[\bar{H}_c\gamma^\mu\gamma_5\tau_a H_c] + \text{C.c.}) + \ldots, \quad (9) \end{aligned}$$

$$\begin{aligned} \mathcal{L}_{2H2H_c}^{(2,q)} = &\, D_1^q([\text{Tr}[(D^\mu H)\gamma_\mu\gamma_5(D^\nu \bar{H})]\text{Tr}[\bar{H}_c\gamma_\nu\gamma_5 H_c] + \text{H.c.}] + \text{C.c.}) + D_2^q(\text{Tr}[(D^\mu H)\gamma_\mu\gamma_5 \bar{H}]\text{Tr}[(D^\nu \bar{H}_c)\gamma_\nu\gamma_5 H_c] + \text{C.c.}) \\ &+ D_3^q(\text{Tr}[(D^\mu H)\gamma_\mu\gamma_5 \bar{H}]\text{Tr}[\bar{H}_c\gamma_\nu\gamma_5(D^\nu H_c)] + \text{H.c.}) + D_4^q([\text{Tr}[(D^\mu D^\nu H)\gamma_\mu\gamma_5 \bar{H}]\text{Tr}[\bar{H}_c\gamma_\nu\gamma_5 H_c] + \text{H.c.}] + \text{C.c.}) \\ &+ E_1^q([\text{Tr}[(D^\mu H)\gamma_\mu\gamma_5\tau^a(D^\nu \bar{H})]\text{Tr}[\bar{H}_c\gamma_\nu\gamma_5\tau_a H_c] + \text{H.c.}] + \text{C.c.}) + \ldots, \quad (10) \end{aligned}$$

where

$$\chi_\pm = \xi^\dagger \chi \xi^\dagger \pm \xi \chi \xi, \qquad \chi = m_\pi^2. \qquad (11)$$

In the above Lagrangians, H.c. and C.c. stand for Hermitian conjugation and charge conjugation, respectively. Notice that the finite parts of the above Lagrangians could also contribute to the potentials, however they will bring a large number of LECs.

In present work, we will adopt Weinberg's scheme [21,22]. Our previous works [50,51] have already applied Weinberg's power counting scheme to investigate the $\bar{B}\bar{B}$ and DD^* systems. The scheme states that with the standard power counting scheme, one first calculates effective potentials [the sum of the two-particle irreducible (2PI) diagrams], then uses them to solve the Lippmann-Schwinger or Schrödinger equation, so complete contributions containing the two-particle reducible (2PR)

diagrams can be retrieved. Here we refer to Refs. [50,51] for more details.

III. POTENTIALS OF THE $D\bar{D}^*$ SYSTEM IN HMChEFT

We will investigate four channels in the $D\bar{D}^*$ system: C parity $C = \pm 1$ and isospin $I = 0$, 1. Therefore we consider the following flavor wave functions [59–62]:

$$
\begin{aligned}
|0,0\rangle &= \frac{1}{2}[(|D^0\bar{D}^{*0}\rangle + |D^+D^{*-}\rangle) \\
&\quad + c(|D^{*0}\bar{D}^0\rangle + |D^{*+}D^-\rangle)], \\
|1,0\rangle &= \frac{1}{2}[(|D^0\bar{D}^{*0}\rangle - |D^+D^{*-}\rangle) \\
&\quad + c(|D^{*0}\bar{D}^0\rangle - |D^{*+}D^-\rangle)], \\
|1,1\rangle &= \frac{1}{\sqrt{2}}(|D^+\bar{D}^{*0}\rangle + c|D^{*+}\bar{D}^0\rangle), \\
|1,-1\rangle &= \frac{1}{\sqrt{2}}(|D^{*0}D^-\rangle + c|D^0D^{*-}\rangle), \quad (12)
\end{aligned}
$$

where the parameter $c = \mp$ stands for $C = \pm 1$.

We first calculate the elastic scattering amplitudes in the processes $D\bar{D}^* \to D\bar{D}^*$ with the defined $D\bar{D}^*$ states (12). Here the contributions up to $O(\epsilon^2)$ are considered. According to the chiral Lagrangians in the previous section, there exist tree-level contact and OPE diagrams at the lowest order $O(\epsilon^0)$. While at $O(\epsilon^2)$, there emerge one-loop diagrams carrying contact interactions, one-loop OPE and TPE diagrams.

Let us focus on the order $O(\epsilon^0)$ first. At $O(\epsilon^0)$, there are two tree-level diagrams which are depicted in Fig. 1. Obviously, Fig. 1(a) stands for a contact contribution while Fig. 1(b) stands for a OPE contribution.

Here we stress that in our depicted diagrams (such as in Fig. 1), the (double-)solid line stands for $D(D^*)$ as well as antiparticle $\bar{D}(\bar{D}^*)$, depending on the concrete term in the expanded isospin amplitude $\langle I, 0|T|I, 0\rangle$, where $|I, 0\rangle$ is defined in Eq. (12). Notice that we label the momenta of the external fields as p_1 for initial D, p_2 for initial $\bar{D}^*$, p_3 for final D and $\bar{D}$, and p_4 for final D^* and $\bar{D}^*$.

At this order, we use the following Lagrangians: the $O(\epsilon^1)$ Lagrangian (1) that depicts the $DD^*\pi$ vertex, the
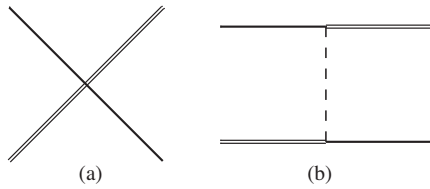
FIG. 1. Tree-level diagrams of the $D\bar{D}^*$ system at $O(\epsilon^0)$. The solid, double-solid, and dashed lines stand for D (or $\bar{D}$), D^* (or $\bar{D}^*$), and π, respectively.

$O(\epsilon^1)$ Lagrangian (5) describing the $\bar{D}\bar{D}^*\pi$ vertex, and the $O(\epsilon^0)$ contact $DD^*\bar{D}\bar{D}^*$ Lagrangian (7). Consequently, the contact amplitudes for the diagram of Fig. 1(a) are calculated to be

$$
\mathcal{M}_{(a)}^{(0)} = 4(D_a + 3E_a - cD_b - 3cE_b)\varepsilon(p_2)\cdot\varepsilon^*(p_4) \text{ for } I = 0,
$$
$$(13)$$

$$
\mathcal{M}_{(a)}^{(0)} = 4(D_a - E_a - cD_b + cE_b)\varepsilon(p_2)\cdot\varepsilon^*(p_4) \text{ for } I = 1.
$$
$$(14)$$

The OPE contributions of Fig. 1(b) read

$$
\mathcal{M}_{(b)}^{(0)} = 3c\frac{g^2}{f^2}\frac{1}{p^2 - m^2}p\cdot\varepsilon(p_2)p\cdot\varepsilon^*(p_4) \text{ for } I = 0, \quad (15)
$$

$$
\mathcal{M}_{(b)}^{(0)} = -c\frac{g^2}{f^2}\frac{1}{p^2 - m^2}p\cdot\varepsilon(p_2)p\cdot\varepsilon^*(p_4) \text{ for } I = 1. \quad (16)
$$

In the above expressions, $p = p_1 - p_4$ denotes the momentum transfer, the superscript (0) of $\mathcal{M}$ stands for the chiral order $O(\epsilon^0)$. The parameter c appearing in $\mathcal{M}$ has been defined in Eq. (12), which takes ∓ 1 for $C = \pm 1$.

Then, we consider the contributions at order $O(\epsilon^2)$, which are illustrated in Figs. 2–4. We can see that there are three types of the diagrams. The diagrams in Fig. 2 all carry $O(\epsilon^0)$ contact interactions, which can be treated as one-loop corrections to Fig. 1(a). In Fig. 3, the diagrams all
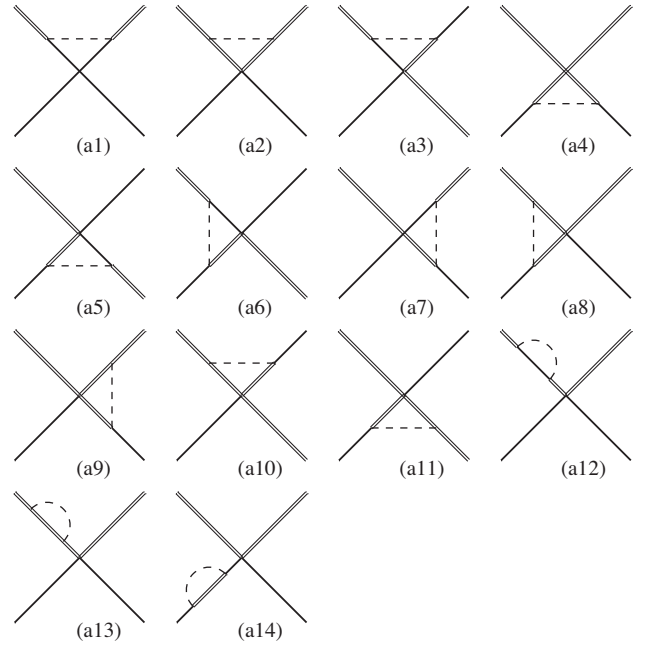
FIG. 2. Diagrams carrying contact interactions at $O(\epsilon^2)$. The solid, double-solid, and dashed lines stand for D (or $\bar{D}$), D^* (or $\bar{D}^*$), and π, respectively.
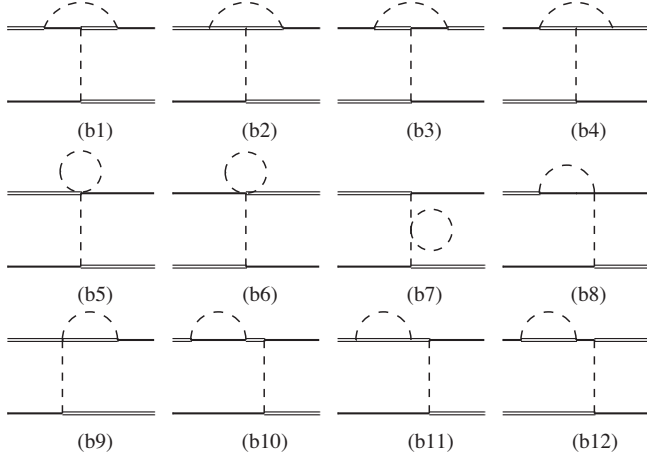
FIG. 3. OPE diagrams at $O(\epsilon^2)$. The solid, double-solid, and dashed lines stand for D (or $\bar{D}$), D^* (or $\bar{D}^*$), and π, respectively.

contribute to OPE interactions, which are just one-loop corrections to Fig. 1(b). Besides the above contributions, there appears to be a new type of diagrams at this order: TPE interactions. They are shown in Fig. 4.

Notice that Figs. 2–4 may only represent typical diagrams having different topologies. For example, each diagram shown in Fig. 2 represents both direct channel $D\bar{D}^* \to D\bar{D}^*$ and cross channel $D\bar{D}^* \to \bar{D}D^*$. The combination of these two channels depends on the specific isospin amplitude $\langle I, 0|T|I, 0\rangle$, where the direct channel and cross channel generally both appear. Formally, the typical diagrams in Figs. 2–4 are the same as those in the doubly charmed system DD^* investigated in our previous work [51], i.e., both the systems have the same topology in Feynman diagrams. Although, there is no cross channel in the DD^* system.

We now focus on the $O(\epsilon^2)$ contribution carrying contact interactions first (Fig. 2). Involved vertexes are the $O(\epsilon^0)$ contact interaction (7), $O(\epsilon^1)$ $DD^*\pi$ interaction (1) and $O(\epsilon^1)$ $\bar{D}\bar{D}^*\pi$ interaction (5). Combined with the defined flavor wave functions (12), their isospin amplitudes can be written as
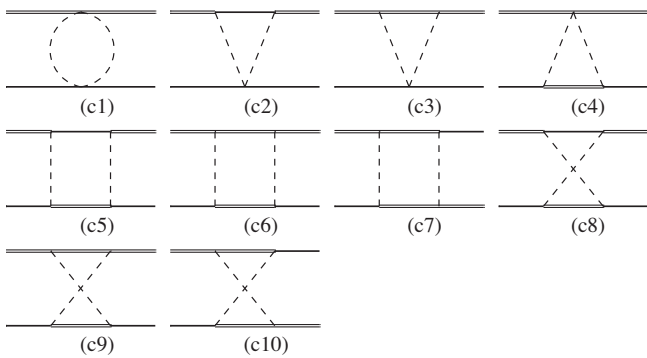
FIG. 4. TPE diagrams at $O(\epsilon^2)$. The solid, double-solid, and dashed lines stand for D (or $\bar{D}$), D^* (or $\bar{D}^*$), and π, respectively.

$$\mathcal{M}^{(2)}_{(a1)} = -4\frac{g^2}{f^2}g_{s1}(A_0 - cA_1)J^g_{22}\varepsilon \cdot \varepsilon^*, \qquad (17)$$

$$\mathcal{M}^{(2)}_{(a2)} = -4(-3+d)(-2+d)\frac{g^2}{f^2}(A_0g_{s1} - cA_1g_{s5})J^g_{22}\varepsilon \cdot \varepsilon^*, \qquad (18)$$

$$\mathcal{M}^{(2)}_{(a3)} = -4\frac{g^2}{f^2}(A_0 - cA_1)g_{s5}J^g_{22}\varepsilon \cdot \varepsilon^*, \qquad (19)$$

$$\mathcal{M}^{(2)}_{(a4)} = -4\frac{g^2}{f^2}(-A_0g_{s1} + dA_0g_{s1} - cA_1g_{s1} + 2cA_1g_{s5}$$
$$- cdA_1g_{s5})J^g_{22}\varepsilon \cdot \varepsilon^*, \qquad (20)$$

$$\mathcal{M}^{(2)}_{(a5)} = -4\frac{g^2}{f^2}(A_0 - cA_1)g_{s5}J^g_{22}\varepsilon \cdot \varepsilon^*, \qquad (21)$$

$$\mathcal{M}^{(2)}_{(a6)} = -4\frac{g^2}{f^2}(A_0g_{s5} - cA_1g_{s1})J^h_{22}\varepsilon \cdot \varepsilon^*, \qquad (22)$$

$$\mathcal{M}^{(2)}_{(a7)} = -4\frac{g^2}{f^2}(A_0g_{s5} - cA_1g_{s1})J^h_{22}\varepsilon \cdot \varepsilon^*, \qquad (23)$$

$$\mathcal{M}^{(2)}_{(a8)} = -4(d-3)(d-2)\frac{g^2}{f^2}(A_0 + cA_1)g_{s5}J^h_{22}\varepsilon \cdot \varepsilon^*, \qquad (24)$$

$$\mathcal{M}^{(2)}_{(a9)} = -4(d-3)(d-2)\frac{g^2}{f^2}(A_0 + cA_1)g_{s5}J^h_{22}\varepsilon \cdot \varepsilon^*, \qquad (25)$$

$$\mathcal{M}^{(2)}_{(a10)} = -4(d-3)(d-2)\frac{g^2}{f^2}(A_0 + cA_1)g_{s5}J^g_{22}\varepsilon \cdot \varepsilon^*, \qquad (26)$$

$$\mathcal{M}^{(2)}_{(a11)} = -4(d-3)(d-2)\frac{g^2}{f^2}(A_0 + cA_1)g_{s5}J^g_{22}\varepsilon \cdot \varepsilon^*, \qquad (27)$$

$$\mathcal{M}^{(2)}_{(a12+13)} = -\frac{3}{2}\frac{g^2}{f^2}(A_0g_{s1} - cA_1g_{s5})[(d-2)\partial_\omega J^b_{22}(\omega_1)$$
$$+ \partial_\omega J^b_{22}(\omega_2)]\varepsilon \cdot \varepsilon^*, \qquad (28)$$

$$\mathcal{M}^{(2)}_{(a14)} = -\frac{3}{2}(d-1)\frac{g^2}{f^2}(A_0g_{s1} - cA_1g_{s5})\partial_\omega J^b_{22}\varepsilon \cdot \varepsilon^*. \qquad (29)$$

In the above, c still takes $\mp$ for $C = \pm$. d is the space-time dimension coming from the dimensional regularization. A_0 and A_1 are constants depending on different diagrams and isospin I, which are collected in Table I. Also, in these expressions ε and ε^* are the abbreviations of the polarization vectors $\varepsilon(p_2)$ and $\varepsilon^*(p_4)$, respectively. Each J is a loop function defined in Refs. [50,51]. For the following OPE and TPE amplitudes these notations apply.

Notice that, one should further expand these amplitudes (17)–(29), later the variables g_{si} and g_{fi} (embed in the constants A_i) in them have to be replaced as the following:

TABLE I.   The constants appearing in the amplitudes (17)–(29).

| | $I=0$ | | $I=1$ | | | |
	A_0	A_1	A_0	A_1	ω_1	ω_2
A_{a1}	$\frac{3}{4}(g_{f1}-g_{f\lambda})$	$\frac{3}{4}(g_{f1}-g_{f\lambda})$	$\frac{3}{4}g_{f1}+\frac{1}{4}g_{f\lambda}$	$-\frac{1}{4}g_{f1}+\frac{5}{4}g_{f\lambda}$	δ	δ
A_{a2}	$\frac{3}{4}(g_{f1}-g_{f\lambda})$	$\frac{3}{4}(g_{f1}-g_{f\lambda})$	$\frac{3}{4}g_{f1}+\frac{1}{4}g_{f\lambda}$	$-\frac{1}{4}g_{f1}+\frac{5}{4}g_{f\lambda}$	0	0
A_{a3}	$\frac{3}{4}(g_{f1}-g_{f\lambda})$	$\frac{3}{4}(g_{f1}-g_{f\lambda})$	$-\frac{1}{4}g_{f1}+\frac{5}{4}g_{f\lambda}$	$\frac{3}{4}g_{f1}+\frac{1}{4}g_{f\lambda}$	δ	$-\delta$
A_{a4}	$\frac{3}{4}(g_{f1}-g_{f\lambda})$	$\frac{3}{4}(g_{f1}-g_{f\lambda})$	$\frac{3}{4}g_{f1}+\frac{1}{4}g_{f\lambda}$	$-\frac{1}{4}g_{f1}+\frac{5}{4}g_{f\lambda}$	$-\delta$	$-\delta$
A_{a5}	$\frac{3}{4}(g_{f1}-g_{f\lambda})$	$\frac{3}{4}(g_{f1}-g_{f\lambda})$	$-\frac{1}{4}g_{f1}+\frac{5}{4}g_{f\lambda}$	$\frac{3}{4}g_{f1}+\frac{1}{4}g_{f\lambda}$	$-\delta$	δ
A_{a6}	$\frac{3}{4}g_{f1}+\frac{9}{4}g_{f\lambda}$	$\frac{3}{4}g_{f1}+\frac{9}{4}g_{f\lambda}$	$\frac{1}{4}(-g_{f1}+g_{f\lambda})$	$\frac{1}{4}(-g_{f1}+g_{f\lambda})$	δ	$-\delta$
A_{a7}	$\frac{3}{4}g_{f1}+\frac{9}{4}g_{f\lambda}$	$\frac{3}{4}g_{f1}+\frac{9}{4}g_{f\lambda}$	$\frac{1}{4}(-g_{f1}+g_{f\lambda})$	$\frac{1}{4}(-g_{f1}+g_{f\lambda})$	$-\delta$	δ
A_{a8}	$\frac{3}{4}g_{f1}+\frac{9}{4}g_{f\lambda}$	$\frac{3}{4}g_{f1}+\frac{9}{4}g_{f\lambda}$	$\frac{1}{4}(-g_{f1}+g_{f\lambda})$	$\frac{1}{4}(-g_{f1}+g_{f\lambda})$	0	$-\delta$
A_{a9}	$\frac{3}{4}g_{f1}+\frac{9}{4}g_{f\lambda}$	$\frac{3}{4}g_{f1}+\frac{9}{4}g_{f\lambda}$	$\frac{1}{4}(-g_{f1}+g_{f\lambda})$	$\frac{1}{4}(-g_{f1}+g_{f\lambda})$	$-\delta$	0
A_{a10}	$\frac{3}{4}(g_{f1}-g_{f\lambda})$	$\frac{3}{4}(g_{f1}-g_{f\lambda})$	$-\frac{1}{4}g_{f1}+\frac{5}{4}g_{f\lambda}$	$\frac{3}{4}g_{f1}+\frac{1}{4}g_{f\lambda}$	0	$-\delta$
A_{a11}	$\frac{3}{4}(g_{f1}-g_{f\lambda})$	$\frac{3}{4}(g_{f1}-g_{f\lambda})$	$-\frac{1}{4}g_{f1}+\frac{5}{4}g_{f\lambda}$	$\frac{3}{4}g_{f1}+\frac{1}{4}g_{f\lambda}$	$-\delta$	0
A_{a12+13}	$g_{f1}+3g_{f\lambda}$	$g_{f1}+3g_{f\lambda}$	$g_{f1}-g_{f\lambda}$	$g_{f1}-g_{f\lambda}$	0	δ
A_{a14}	$g_{f1}+3g_{f\lambda}$	$g_{f1}+3g_{f\lambda}$	$g_{f1}-g_{f\lambda}$	$g_{f1}-g_{f\lambda}$	$-\delta$	$-$

$$g_{s1}g_{f1} \to D_a, \qquad g_{s5}g_{f1} \to D_b,$$
$$g_{s1}g_{f\lambda} \to E_a, \qquad g_{s5}g_{f\lambda} \to E_b. \tag{30}$$

Then we consider the OPE contribution showing in Fig. 3. To describe the $O(\epsilon^1)$ $DD^*\pi$, $DD^*3\pi$, $\bar{D}\bar{D}^*\pi$, and $\bar{D}\bar{D}^*3\pi$ vertexes, we utilize the chiral Lagrangians (1) and (5). According to the flavor wave functions (12) corresponding isospin amplitudes are

$$\mathcal{M}^{(2)}_{(b1)} = -4cA\frac{g^4}{f^4}J^g_{22}\frac{p\cdot\varepsilon p\cdot\varepsilon^*}{p^2-m^2}, \tag{31}$$

$$\mathcal{M}^{(2)}_{(b2)} = 4c(d-3)(d-2)A\frac{g^4}{f^4}J^g_{22}\frac{p\cdot\varepsilon p\cdot\varepsilon^*}{p^2-m^2}, \tag{32}$$

$$\mathcal{M}^{(2)}_{(b3)} = -4cA\frac{g^4}{f^4}J^g_{22}\frac{p\cdot\varepsilon p\cdot\varepsilon^*}{p^2-m^2}, \tag{33}$$

$$\mathcal{M}^{(2)}_{(b4)} = 4c(d-3)(d-2)A\frac{g^4}{f^4}J^g_{22}\frac{p\cdot\varepsilon p\cdot\varepsilon^*}{p^2-m^2}, \tag{34}$$

$$\mathcal{M}^{(2)}_{(b5)} = 4cA\frac{g^2}{f^4}J^c_0\frac{p\cdot\varepsilon p\cdot\varepsilon^*}{p^2-m^2}, \tag{35}$$

$$\mathcal{M}^{(2)}_{(b6)} = 4cA\frac{g^2}{f^4}J^c_0\frac{p\cdot\varepsilon p\cdot\varepsilon^*}{p^2-m^2}, \tag{36}$$

$$\mathcal{M}^{(2)}_{(b7)} = 4cA\frac{g^2}{f^2}\left[\frac{2}{3f^2}\left(2m^2L+\frac{2m^2}{16\pi^2}\log\left(\frac{m}{\mu}\right)\right)\right]\frac{p\cdot\varepsilon p\cdot\varepsilon^*}{p^2-m^2}, \tag{37}$$

$$\mathcal{M}^{(2)}_{(b8)} = 0, \tag{38}$$

$$\mathcal{M}^{(2)}_{(b9)} = 0, \tag{39}$$

$$\mathcal{M}^{(2)}_{(b10+11)} = -\frac{3}{2}cA\frac{g^4}{f^4}[(d-2)\partial_\omega J^b_{22}(\omega_1) + \partial_\omega J^b_{22}(\omega_2)]$$
$$\times\frac{p\cdot\varepsilon p\cdot\varepsilon^*}{p^2-m^2}, \tag{40}$$

$$\mathcal{M}^{(2)}_{(b12)} = -\frac{3}{2}cA\frac{g^4}{f^4}(d-1)\partial_\omega J^b_{22}\frac{p\cdot\varepsilon p\cdot\varepsilon^*}{p^2-m^2}, \tag{41}$$

$$\mathcal{M}^{(2)}_{f^{(2)}} = 4cA\frac{g^2}{f^2}\left[\frac{2}{f^2}\left(2m^2L+\frac{2m^2}{16\pi^2}\log\left(\frac{m}{\mu}\right)\right)\right]\frac{p\cdot\varepsilon p\cdot\varepsilon^*}{p^2-m^2}, \tag{42}$$

where A is a constant depending on each diagram and isospin I, and we collect them in Table II. Note that in Eq. (42), $\mathcal{M}_{f^{(2)}}$ stands for the tree-level OPE amplitude [Eqs. (15) or (16)] where the pion decay constant f has to be replaced by its $O(\epsilon^2)$ correction $f^{(2)}$.

Final piece is the TPE contribution depicted in Fig. 4. Here we need $O(\epsilon^1)$ $DD^*\pi$, $DD^*2\pi$, $\bar{D}\bar{D}^*\pi$, and $\bar{D}\bar{D}^*2\pi$ vertexes. Using the chiral Lagrangians (1) and (5), the isospin amplitudes of the TPE are written by

$$\mathcal{M}^{(2)}_{(c1)} = -4\frac{1}{f^4}[q_0^2A_5J^F_0 - q_0^2(A_{15}+A_{51}-2A_5)J^F_{11}$$
$$+ q_0^2(A_1 - A_{15} - A_{51} + A_5)J^F_{21}$$
$$+ (A_1 - A_{15} - A_{51} + A_5)J^F_{22}]\varepsilon\cdot\varepsilon^*, \tag{43}$$

$$\mathcal{M}^{(2)}_{(c2)} = 4i\frac{g^2}{f^4}[-q_0 A_5 J^S_{21} + q_0(A_1 - A_5)J^S_{31} + (A_1 - A_5)J^S_{34}]\varepsilon \cdot \varepsilon^*$$

$$+ 4i\frac{g^2}{f^4}[-q_0 A_5 J^S_{11} + q_0(A_1 - 2A_5)J^S_{22} + (A_1 - A_5)J^S_{24} + q_0(A_1 - A_5)J^S_{32} + (A_1 - A_5)J^S_{33}]q \cdot \varepsilon q \cdot \varepsilon^*, \quad (44)$$

$$\mathcal{M}^{(2)}_{(c3)} = -4i(d-3)\frac{g^2}{f^4}[-q_0\vec{q}^2 A_5 J^S_{11} + (d-2)q_0 A_5 J^S_{21} + q_0\vec{q}^2(A_1 - 2A_5)J^S_{22} + \vec{q}^2(A_1 - A_5)J^S_{24} - (d-2)q_0(A_1 - A_5)J^S_{31}$$

$$+ q_0\vec{q}^2(A_1 - A_5)J^S_{32} + \vec{q}^2(A_1 - A_5)J^S_{33} - (d-2)(A_1 - A_5)J^S_{34}]\varepsilon \cdot \varepsilon^*$$

$$- 4i(d-3)\frac{g^2}{f^4}[-q_0 A_5 J^S_{11} + q_0(A_1 - 2A_5)J^S_{22} + (A_1 - A_5)J^S_{24} + q_0(A_1 - A_5)J^S_{32} + (A_1 - A_5)J^S_{33}]q \cdot \varepsilon q \cdot \varepsilon^*, \quad (45)$$

$$\mathcal{M}^{(2)}_{(c4)} = -4i\frac{g^2}{f^4}[-q_0\vec{q}^2 A_5 J^T_{11} + (d-1)q_0 A_5 J^T_{21} + q_0\vec{q}^2(A_1 - 2A_5)J^T_{22} + \vec{q}^2(A_1 - A_5)J^T_{24} - (d-1)q_0(A_1 - A_5)J^T_{31}$$

$$+ q_0\vec{q}^2(A_1 - A_5)J^T_{32} + \vec{q}^2(A_1 - A_5)J^T_{33} - (d-1)(A_1 - A_5)J^T_{34}]\varepsilon \cdot \varepsilon^*, \quad (46)$$

$$\mathcal{M}^{(2)}_{(c5)} = -4A_1\frac{g^4}{f^4}[\vec{q}^2 J^B_{31} - (d+1)J^B_{41} + \vec{q}^2 J^B_{42}]\varepsilon \cdot \varepsilon^*$$

$$+ 4A\frac{g^4}{f^4}[J^B_{21} - \vec{q}^2 J^B_{22} + (d+3)J^B_{31} - 2\vec{q}^2 J^B_{32} + (d+3)J^B_{42} - \vec{q}^2 J^B_{43}]q \cdot \varepsilon q \cdot \varepsilon^*, \quad (47)$$

$$\mathcal{M}^{(2)}_{(c6)} = 4A_1(d-3)\frac{g^4}{f^4}[-\vec{q}^2 J^B_{21} + \vec{q}^4 J^B_{22} - (2d+1)\vec{q}^2 J^B_{31} + 2\vec{q}^4 J^B_{32} + (d-2)(d+1)J^B_{41} - (2d+1)\vec{q}^2 J^B_{42} + \vec{q}^4 J^B_{43}]\varepsilon \cdot \varepsilon^*$$

$$- 4A(d-3)\frac{g^4}{f^4}[J^B_{21} - \vec{q}^2 J^B_{22} + (d+3)J^B_{31} - 2\vec{q}^2 J^B_{32} + (d+3)J^B_{42} - \vec{q}^2 J^B_{43}]q \cdot \varepsilon q \cdot \varepsilon^*, \quad (48)$$

$$\mathcal{M}^{(2)}_{(c7)} = -4cA_1(d-3)\frac{g^4}{f^4}J^B_{21}(\vec{p}^2\varepsilon \cdot \varepsilon^* + p \cdot \varepsilon p \cdot \varepsilon^*), \quad (49)$$

$$\mathcal{M}^{(2)}_{(c8)} = -4A_1\frac{g^4}{f^4}[\vec{q}^2 J^R_{31} - (d+1)J^R_{41} + \vec{q}^2 J^R_{42}]\varepsilon \cdot \varepsilon^*$$

$$+ 4A\frac{g^4}{f^4}[J^R_{21} - \vec{q}^2 J^R_{22} + (d+3)J^R_{31} - 2\vec{q}^2 J^R_{32} + (d+3)J^R_{42} - \vec{q}^2 J^R_{43}]q \cdot \varepsilon q \cdot \varepsilon^*, \quad (50)$$

$$\mathcal{M}^{(2)}_{(c9)} = 4A_1(d-3)\frac{g^4}{f^4}[-\vec{q}^2 J^R_{21} + \vec{q}^4 J^R_{22} - (2d+1)\vec{q}^2 J^R_{31} + 2\vec{q}^4 J^R_{32} + (d-2)(d+1)J^R_{41} - (2d+1)\vec{q}^2 J^R_{42} + \vec{q}^4 J^R_{43}]\varepsilon \cdot \varepsilon^*$$

$$- 4A(d-3)\frac{g^4}{f^4}[J^R_{21} - \vec{q}^2 J^R_{22} + (d+3)J^R_{31} - 2\vec{q}^2 J^R_{32} + (d+3)J^R_{42} - \vec{q}^2 J^R_{43}]q \cdot \varepsilon q \cdot \varepsilon^*, \quad (51)$$

TABLE II. The constants A (as well as $\omega_{1,2}$) appearing in the OPE amplitudes (31)–(42).

	A_{b1}	A_{b2}	A_{b3}	A_{b4}	A_{b5}	A_{b6}	A_{b7}	A_{b8}	A_{b9}	A_{b10+11}	A_{b12}	$A_{f(2)}$
$I=0$	$-\frac{3}{16}$	$-\frac{3}{16}$	$-\frac{3}{16}$	$-\frac{3}{16}$	$-\frac{1}{4}$	$-\frac{1}{4}$	$\frac{3}{4}$	—	—	$\frac{3}{4}$	$\frac{3}{4}$	$\frac{3}{4}$
$I=1$	$\frac{1}{16}$	$\frac{1}{16}$	$\frac{1}{16}$	$\frac{1}{16}$	$\frac{1}{12}$	$\frac{1}{12}$	$-\frac{1}{4}$	—	—	$-\frac{1}{4}$	$-\frac{1}{4}$	$-\frac{1}{4}$
ω_1	δ	0	$-\delta$	$-\delta$	—	—	—	—	—	0	$-\delta$	—
ω_2	$-\delta$	$-\delta$	δ	0	—	—	—	—	—	δ	—	—

TABLE III.   The constants appearing in the TPE amplitudes (43)–(52). Note that we have $A_{51} = A_{15}$.

	$I = 0$			$I = 1$				
	A_1	A_5	A_{15}	A_1	A_5	A_{15}	ω_1	ω_2
A_{c1}	$\frac{3}{16}$	$\frac{3}{16}$	$\frac{-3}{16}$	$\frac{-1}{16}$	$\frac{-1}{16}$	$\frac{1}{16}$	–	–
A_{c2}	$\frac{-3i}{8}$	$\frac{3i}{8}$	–	$\frac{i}{8}$	$\frac{-i}{8}$	–	δ	–
A_{c3}	$\frac{-3i}{8}$	$\frac{3i}{8}$	–	$\frac{i}{8}$	$\frac{-i}{8}$	–	0	–
A_{c4}	$\frac{3i}{8}$	$\frac{-3i}{8}$	–	$\frac{-i}{8}$	$\frac{i}{8}$	–	$-\delta$	–
A_{c5}	$\frac{9}{16}$	–	–	$\frac{1}{16}$	–	–	$-\delta$	δ
A_{c6}	$\frac{9}{16}$	–	–	$\frac{1}{16}$	–	–	$-\delta$	0
A_{c7}	$\frac{9}{16}$	–	–	$\frac{1}{16}$	–	–	$-\delta$	0
A_{c8}	$\frac{-3}{16}$	–	–	$\frac{5}{16}$	–	–	$-\delta$	δ
A_{c9}	$\frac{-3}{16}$	–	–	$\frac{5}{16}$	–	–	$-\delta$	0
A_{c10}	$\frac{-3}{16}$	–	–	$\frac{5}{16}$	–	–	$-\delta$	$-\delta$

$$\mathcal{M}^{(2)}_{(c10)} = 4cA_1(d-3)\frac{g^4}{f^4}J^R_{21}(\vec{p}^2\varepsilon \cdot \varepsilon^* + p \cdot \varepsilon p \cdot \varepsilon^*), \quad (52)$$

where A_1, A_5, A_{15}, and A_{51} are constants collected in Table III.

Notice that in the above amplitudes (17)–(52), the loop functions $J^{a/b}_{ij}(m,\omega)$, $J^{g/h}_{ij}(m,\omega_1,\omega_2)$, $J^F_{ij}(m_1,m_2,q)$, $J^{T/S}_{ij}(m_1,m_2,\omega,q)$, and $J^{R/B}_{ij}(m_1,m_2,\omega_1,\omega_2,q)$ are abbreviated as $J^{a/b}_{ij}$, $J^{g/h}_{ij}$, J^F_{ij}, $J^{T/S}_{ij}$, and $J^{R/B}_{ij}$, respectively. The corresponding constants ω_1 and ω_2 for different diagrams are listed in Tables I–III. These loop functions J are calculated using dimensional regularization, with the modified minimal subtraction scheme.

Besides the one loop diagrams in Figs. 2–4, at this order $O(\epsilon^2)$ tree-level amplitudes also emerge. For example, there are $O(\epsilon^2)$ contact contributions that come from the $O(\epsilon^2)$ contact Lagrangians (8)–(10). The LECs in Eqs. (8)–(10) actually consist of two parts: the finite parts that will induce large amounts of unknown parameters, and the divergent parts which are used to renormalize the $O(\epsilon^2)$ one-loop diagrams. In this work, the finite parts of the LECs in Eqs. (8)–(10) are ignored due to the lack of fitting data available.

In our work, we consider S-wave interactions, therefore we have the following substitutions for the terms related to the polarization vectors:

$$\vec{\varepsilon} \cdot \vec{\varepsilon}^* \rightarrowtail 1, \quad (53)$$

$$\vec{\varepsilon} \cdot \vec{p}\vec{\varepsilon}^* \cdot \vec{p} \rightarrowtail \frac{1}{d-1}\vec{p}^2. \quad (54)$$

After calculating the scattering amplitudes of the $D\bar{D}^*$ system in the four channels, the $D\bar{D}^*$ potentials in momentum space can be obtained via the relation:

$$\mathcal{V} = -\frac{\mathcal{M}}{\sqrt{\prod 2M_i \prod 2M_f}}. \quad (55)$$

Note that in Eqs. (17)–(52), we did not show the factor $\prod M_i \prod M_f$.

In this work, we aim to investigate whether the $D\bar{D}^*$ interactions are strong enough to form molecular states, therefore we are interested in the $D\bar{D}^*$ potentials at coordinate space. With the help of Fourier transformation we can get the potential $\mathcal{V}(\mathbf{r})$:

$$\mathcal{V}(\mathbf{r}) = \int \frac{d\mathbf{p}}{(2\pi)^3}\mathcal{V}(\mathbf{p})e^{i\mathbf{p}\cdot\mathbf{r}}. \quad (56)$$

Because $\mathcal{V}(\mathbf{p})$ is a polynomial of p, the integral will be highly divergent with the increasing of the order. Here we renormalize the potential by introducing a Gaussian cutoff $\exp(-\vec{p}^{2n}/\Lambda^{2n})$ with $n = 2$ as in Ref. [51].

IV. NUMERICAL RESULTS AND DISCUSSIONS

In this section, we substitute the calculated potentials into the Schrödinger equation and explore whether the $D\bar{D}^*$ interactions are strong enough to form bound states. Later we discuss the behaviors of the $D\bar{D}^*$ potentials $\mathcal{V}(\mathbf{r})$ in detail.

In this work, we use the following parameters: $m_\pi = 0.139$ GeV, the $D - D^*$ mass splitting $\delta = 0.142$ GeV, the decay constant $f_\pi = 0.086$ GeV, the renormalization scale $\mu = 4\pi f$, and the bare coupling constant $g = 0.65$ as in Ref. [51]. In our paper we ignore the isospin breaking in the isospin doublet $(D^{(*)0}, D^{(*)+})$.

For the LECs D_a, D_b, E_a, and E_b in Eq. (7), we lack available data that can be fitted, so we use the resonance saturation to estimate them. With the expressions in Appendix, we obtain $D_a = -13.23, E_a = -11.49, D_b = 0$, and $E_b = 0$.

A. Bound state properties of the $D\bar{D}^*$ system

We first investigate whether the $D\bar{D}^*$ interactions are strong enough to form bound states. The $D\bar{D}^*$ system has the quantum numbers $C = \pm 1$ and $I = 0, 1$; i.e., there are four channels: $I^G(J^{PC}) = 0^+(1^{++})$, $0^-(1^{+-})$, $1^-(1^{++})$, and $1^+(1^{+-})$.

For the reliability of our investigation, we will leave the cutoff parameter Λ undetermined. Generally, Λ is adopted below the ρ meson mass in nucleon-nucleon ChEFT [32]. Also, in our previous work, we used $\Lambda = 0.7$ GeV [51]. In this paper, we will vary the cutoff at the vicinity of 0.7 GeV to search for the bound state solutions, where a relatively wide range will be adopted.

We solve the Schrödinger equations with the $D\bar{D}^*$ potentials $\mathcal{V}(\mathbf{r})$ (56). We present the Λ dependences of calculated masses, binding energies and root-mean-square (rms) radii in Table IV. In Table IV, with Λ ranging from 0.3 to 1.1 GeV, we can see that there are various bound state solutions appearing in the considered channels.

We now discuss the bound state properties in the $0^+(1^{++})$, $0^-(1^{+-})$, $1^-(1^{++})$, and $1^+(1^{+-})$ channels.

1. $0^+(1^{++})$

For the $0^+(1^{++})$ channel, the bound state solution appears at $\Lambda = 0.4$ GeV, its binding energy then becomes deeper with increasing Λ. However it disappears at 1.0 GeV. The binding energy varies from 0.1–8.1 MeV which is within one order of magnitude. As for the rms radius, we can see that except a large radius (9.0 fm) at $\Lambda = 0.4$ GeV, the radius is basically around 2 fm.

In a word, in our HMChEFT calculations, the $D\bar{D}^*$ interaction in the $0^+(1^{++})$ channel is strong enough to form a bound state. In this channel we have a loosely bound state with the mass around 3872 MeV, the binding energy 4–5 MeV and the rms radius about 2 fm. This solution just corresponds to $X(3872)$, so our estimates indicate that $X(3872)$ indeed can be treated as a good candidate of $0^+(1^{++})$ $D\bar{D}^*$ molecular state, or we can say the $D\bar{D}^*$ interaction is strongly responsible for $X(3872)$.

2. $0^-(1^{+-})$

We now focus on the $0^-(1^{+-})$ channel. In Table IV, there exists a shallow bound state solution within only a narrow cutoff range $\Lambda = 0.7$–0.8 GeV. The binding energy E is 0.2–0.3 MeV which is quite small. Consequently, the solution has a large radius with around 7 fm. So we conclude that in the $0^-(1^{+-})$ channel, the binding between $D\bar{D}^*$ is relatively weaker comparing to the $0^+(1^{++})$ discussed above, but their interaction is still strong enough to form a shallow bound state.

3. $1^-(1^{++})$

In this channel, there is no bound state solution in the all range ($\Lambda = 0.3$–1.1 GeV). Combining with the bound state property in the channel $1^+(1^{+-})$ that will be discussed below, we conclude that the $D\bar{D}^*$ interaction in the $1^-(1^{++})$ channel is the weakest among all four channels.

4. $1^+(1^{+-})$

For the $1^+(1^{+-})$ channel, we can find a bound state solution beginning with a relatively large cutoff $\Lambda = 1.0$ GeV. Different from the solutions in previous channels, in this channel, the binding energy just becomes deeper and deeper with increasing Λ. At $\Lambda = 1.0$ GeV, we have the binding energy $E = 13.3$ MeV with the rms radius $r_{\text{rms}} = 1.0$ fm. Because of the large cutoff needed to produce the bound state, we can say that the binding in the $1^+(1^{+-})$ channel is weaker than that in the $0^+(1^{++})$ or $0^-(1^{+-})$ channel. In general, we find that the strongest binding of the $D\bar{D}^*$ system is in the $0^+(1^{++})$ channel, the next is in the $0^-(1^{+-})$ channel, then in the $1^+(1^{+-})$ channel, the final is in the $1^-(1^{++})$ channel.

B. The behaviors of the $D\bar{D}^*$ potentials

In the previous subsections, we explore the bound state properties in the four $D\bar{D}^*$ channels. We find that, with some reasonable cutoffs, there will emerge bound state solutions. In this section, to give a deep understandings of

TABLE IV. The bound state solutions in the four $D\bar{D}^*$ channels. The cutoff parameter Λ, calculated mass M, binding energy E, and rms radius r_{rms} are in units of GeV, MeV, MeV, and fm, respectively.

| Λ | $0^+(1^{++})$ | | | $0^-(1^{+-})$ | | | $1^-(1^{++})$ | | | $1^+(1^{+-})$ | | |
	M	E	r_{rms}	M	E	r_{rms}	M	E	r_{rms}	M	E	r_{rms}
0.3	−	−	−	−	−	−	−	−	−	−	−	−
0.4	3.875.7	0.1	9.0	−	−	−	−	−	−	−	−	−
0.5	3874.4	1.4	3.2	−	−	−	−	−	−	−	−	−
0.6	3872.2	3.6	2.1	−	−	−	−	−	−	−	−	−
0.7	3870.0	5.8	1.8	3875.6	0.2	8.0	−	−	−	−	−	−
0.8	3868.6	7.2	1.6	3875.5	0.3	6.4	−	−	−	−	−	−
0.9	3867.7	8.1	1.5	−	−	−	−	−	−	−	−	−
1.0	−	−	−	−	−	−	−	−	−	3862.5	13.3	1.0
1.1	−	−	−	−	−	−	−	−	−	3813.0	62.8	0.6

the bound state properties and the $D\bar{D}^*$ interactions, we further discuss the behaviors of the $D\bar{D}^*$ potentials $\mathcal{V}(\mathbf{r})$.

Back to Table IV, we see around $\Lambda = 0.6$ GeV the solution in the $0^+(1^{++})$ channel is close to the location of $X(3872)$ most. For a more delicate investigation, here we set the cutoff to be $\Lambda = 0.62$ GeV after fitting the mass of $X(3872)$. With this cutoff we now present $\mathcal{V}(\mathbf{r})$ of all channels in Fig. 5.

For the $0^+(1^{++})$ channel, we see that the OPE contribution and the contribution carrying contact interactions are attractive, where the former is relatively weak. And the TPE contribution provides a strong repulsive force. Our numerical estimate reveals that with the increase of the cutoff Λ, the attractive contributions as well as the repulsive TPE contribution all become stronger, however their cancellation just leads to a stable total potential $\mathcal{V}(\mathbf{r})$.

In the $0^-(1^{+-})$ channel, the behaviors of the TPE contribution and the contribution carrying contact interactions do not differ from those in the $0^+(1^{++})$ channel discussed above, whereas the OPE contribution changes to be repulsive. Thus, they lead to a weaker attraction comparing to the $0^+(1^{++})$ channel. That explains why

the binding energy in this channel is always smaller than that in the $0^+(1^{++})$ channel (see the binding energies in Table IV).

For the $1^-(1^{++})$ channel, the OPE contribution is repulsive while the TPE contribution and the contribution carrying contact interactions are attractive. The cancellation between them makes the line shape of the total $\mathcal{V}(\mathbf{r})$ basically follow the line shape of the potential carrying contact interactions. Observing the amount of the total $\mathcal{V}(\mathbf{r})$, we see that, although attractive, it is not strong enough comparing to the amount in the $0^+(1^{++})$ or $0^-(1^{+-})$ channel.

At the $1^+(1^{+-})$ channel in Fig. 5, all the contributions are attractive. However at the middle range $r = 6$–12 GeV^{-1}, the total $\mathcal{V}(\mathbf{r})$ is repulsive, which originates from the repulsion of the TPE. This causes the attraction of the $1^+(1^{+-})$ channel to be weakened. Indeed, there is no bound state solution at $\Lambda = 0.62$ GeV. Actually, when looking at Table IV we need a considerably high Λ to obtain a bound state solution.

In general, through analyzing the potentials $\mathcal{V}(\mathbf{r})$ depicted in Fig. 5, we have understood the specific
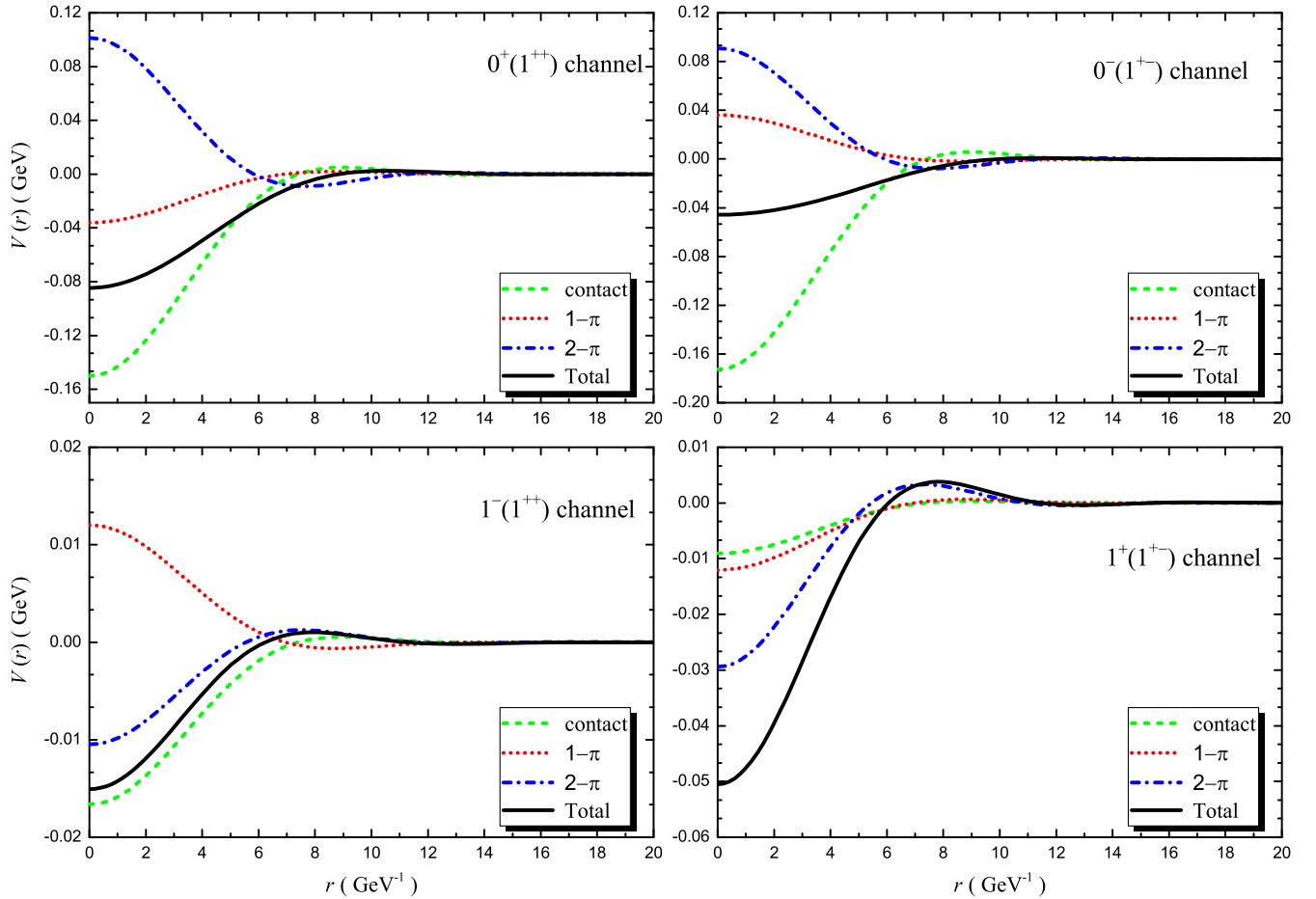
FIG. 5. The potentials $\mathcal{V}(\mathbf{r})$ of the $D\bar{D}^*$ system at $\Lambda = 0.62$ GeV. The label "contact" stands for the contribution carrying contact interactions. Here the $0^+(1^{++})$ channel has a bound state solution with a mass around 3872 MeV.

mechanism of the bound state formation in each channel. Depend on the distinct behaviors of the contribution carrying contact interactions, OPE and TPE contributions in the four channels, the total potentials $\mathcal{V}(\mathbf{r})$ all present attractive line shapes but with different strengths. We find that the most attractive potential is in the $0^+(1^{++})$ channel, then in the $0^-(1^{+-})$ channel, then in the $1^+(1^{+-})$ channel, the final is in the $1^-(1^{++})$ channel.

Combining with the discussions of the bound state properties in Sec. IVA, we conclude that there is a hierarchy of the strengths in the $D\bar{D}^*$ interactions:

$$\text{str.}[0^+(1^{++})] > \text{str.}[0^-(1^{+-})] > \text{str.}[1^+(1^{+-})]$$
$$> \text{str.}[1^-(1^{++})], \tag{57}$$

where str. stands for the strength of the $D\bar{D}^*$ interaction. Note that despite discrepancies in details, this conclusion is consistent with the one-boson-exchange model calculations [20,60,62].

C. $0^-(1^{+-})$ and $1^+(1^{+-})$ molecular states

In previous two sections, we point out the strength ordering in the $D\bar{D}^*$ interactions. But that does not mean they can all produce bound states. From Table IV we already found that only the $0^+(1^{++})$, $0^-(1^{+-})$, and $1^+(1^{+-})$ channels have bound state solutions. In this section we focus on the $0^-(1^{+-})$ and $1^+(1^{+-})$ channels that have no direct experimental indications.

As discussed in Sec. IVA, the solution with the mass around 3872 MeV in the $0^+(1^{++})$ channel just corresponds to $X(3872)$. That means $X(3872)$ has a strong relation to the $D\bar{D}^*$ interaction, in other words, $X(3872)$ is a good candidate of the $0^+(1^{++})$ molecular state. In other two channels $0^-(1^{+-})$ and $1^+(1^{+-})$, $D\bar{D}^*$ also tends to form molecular states.

From Sec. IVA, we have learned that, in the $0^-(1^{+-})$ channel, the shallow bound state solution has the binding energy 0.2–0.3 MeV with $\Lambda = 0.7$–0.8 GeV. Hence we plot the potential $\mathcal{V}(\mathbf{r})$ at $\Lambda = 0.8$ GeV in Fig. 6. From Fig. 6, the OPE and TPE contributions are repulsive, so the binding of the calculated $0^-(1^{+-})$ molecular state is mainly provided by the potential carrying contact interactions. Also, we can see that the attraction is mainly provided in a range round 2–8 GeV^{-1}.

In other channel $1^+(1^{+-})$, we have a molecular state with a considerable binding energy at $\Lambda = 1.0$ GeV. Its potential $\mathcal{V}(\mathbf{r})$ is depicted in Fig. 7. All the contributions are attractive, but the binding is mainly provided by the TPE contribution. Also, it is basically a short range attraction.

In general, the $0^-(1^{+-})$ and $1^+(1^{+-})$ molecular states have different binding mechanisms under the competitions of the contribution carrying contact interactions, OPE and TPE contributions. As we know, the experiment has not observed any possible structures that can fit into our
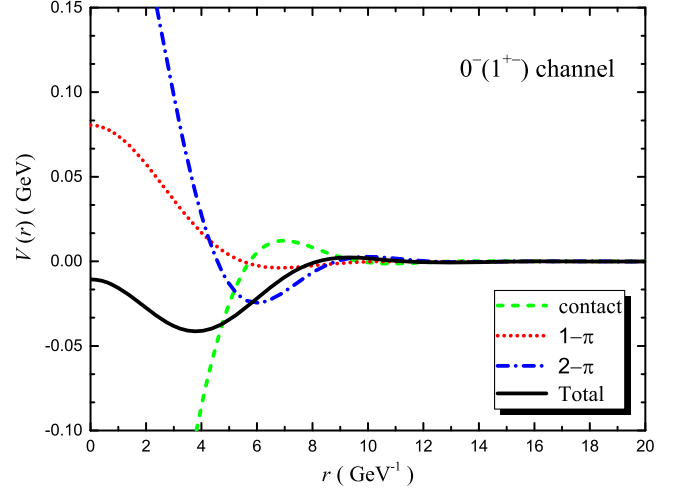
FIG. 6. The potential $\mathcal{V}(\mathbf{r})$ of the $D\bar{D}^*$ system in the $0^-(1^{+-})$ channel at $\Lambda = 0.8$ GeV. The label "contact" stands for the contribution carrying contact interactions. Here this channel has a bound state solution.

predicted $0^-(1^{+-})$ and $1^+(1^{+-})$ molecular candidates yet, so we briefly discuss their discovery potentials in the following.

We first focus on their decay patterns. The $0^-(1^{+-})$ state has possible two body hidden charm decay channels $\eta_c\omega$ and $J/\psi\eta$. It can also have three body strong decays such as $J/\psi\pi^0\pi^0$ and $h_c(1P)\pi\pi$. In other possible channels such as $D^0\bar{D}^{*0}$, $J/\psi\pi^+\pi^-$, and $D^0\bar{D}^0\pi^0$, the signal can be overwhelmed by $X(3872)$. It may also have a baryonic decay channel $p\bar{p}$, radiative decay channels $\gamma\eta_c$, $\gamma\chi_{c0}$ $\gamma\chi_{c1}$, $\gamma\chi_{c2}$, and $\gamma\eta_c(2S)$.

The $1^+(1^{+-})$ state has possible two body hidden charm decay channels $\eta_c\rho$, $J/\psi\pi$, $h_c(1P)\pi$, and $\psi(2S)\pi$, three body decay channels $\eta_c\pi\pi$, $\chi_{c0}\pi\pi$, $\chi_{c1}\pi\pi$, $\chi_{c2}\pi\pi$, a baryonic decay channel $p\bar{p}$, and radiative decay channels $\gamma\eta_c$, $\gamma\chi_{c0}$ $\gamma\chi_{c1}$, $\gamma\chi_{c2}$, and $\gamma\eta_c(2S)$. So it has more decay channels than the $0^-(1^{+-})$ state.

These two possible molecular states can be produced in various production mechanisms. For example, they can be searched in the e^+e^- collisions at the BESIII and Belle II experiments. It is also promising to collect them in the b decay processes, such as $B \to X(0^-(1^{+-})/1^+(1^{+-})) + K$.

In fact, some decay channels listed above have already been measured in experiment. For example, $J/\psi\pi$ is the discovery channel of famous $Z_c(3900)$ [12,13,88,89]. It is possible that our predicted $1^+(1^{+-})$ state is the neutral component of isovector $Z_c(3900)$, although there exists a discrepancy in mass. On the other hand, if the $1^+(1^{+-})$ state is different from $Z_c(3900)$, there may exist more than one enhancement around 3.8–3.9 GeV in the $J/\psi\pi$ invariant mass spectrum. Because of the limited resolution in the invariant mass distributions of Refs. [12,13,88–91], we cannot pin down this issue now. We hope more sophisticated studies in the future can clarify this problem. As for
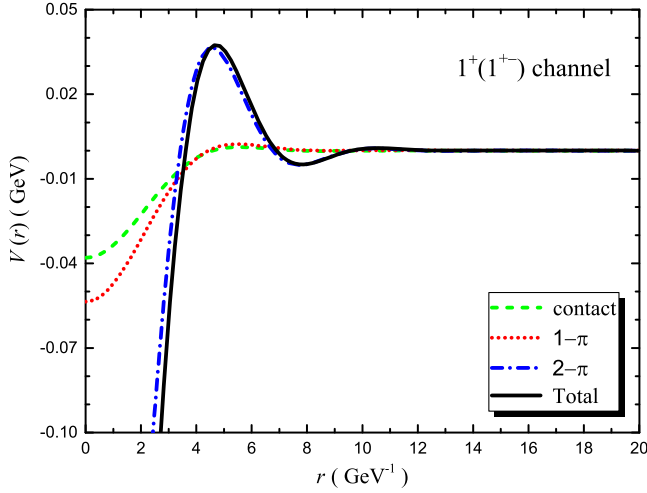
FIG. 7. The potential $\mathcal{V}(\mathbf{r})$ of the $D\bar{D}^*$ system in the $1^+(1^{+-})$ channel at $\Lambda = 1.0$ GeV. The label "contact" stands for the contribution carrying contact interactions. Here this channel has a bound state solution.

the $h_c(1P)\pi$ and $\psi(2S)\pi$ channels, no structure is found around 3.8–3.9 GeV so far.

The $J/\psi\eta$ decay channel of the $0^-(1^{+-})$ molecular state has also been studied in some experiments. In 2004, *BABAR* measured the invariant mass spectrum of the $J/\psi\eta$ in the process $B \to J/\psi\eta K$ [92]. In Fig. 8, we can see that there seems to be a peak around the $D\bar{D}^*$ threshold. In the measurement of Ref. [93], a small enhancement also can be seen in their $J/\psi\eta\eta$ invariant mass spectrum. These enhancements may be related to our predicted $0^-(1^{+-})$ molecular state. In addition, a hint appears in the $\eta_c\omega$ invariant mass spectrum in Ref. [94] too. However, in these experiments the number of the events around this region is limited, we hope experiments can pay more attention on these channels, especially the $J/\psi\eta$ in the future.

In addition, *BABAR* measured a kaon momentum spectrum in $B \to X(c\bar{c}) + K$ [95]. The $X(3872)$ signal is located around 3.8–3.9 GeV. With more refined data in
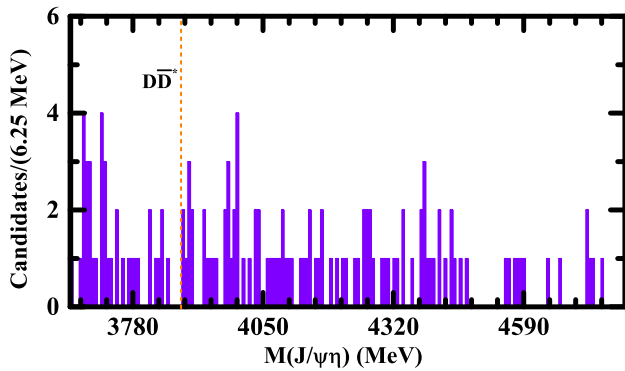
FIG. 8. The $J/\psi\eta$ invariant mass distribution in the process $B \to J/\psi\eta K$, where the data comes from the *BABAR* measurement [92].

the future, we hope there will emerge fine structures if our predicted $0^-(1^{+-})$ and $1^+(1^{+-})$ states exist.

Other production mechanisms such as the low energy $p\bar{p}$ collision at $\bar{P}$ANDA are also promising. The $0^-(1^{+-})$ and $1^+(1^{+-})$ states can be produced through the s or t channel in the $p\bar{p}$ scattering process.

V. SUMMARY

In our previous paper [51], we studied the doubly charmed system DD^* in the framework of HMChEFT. We applied the obtained DD^* chiral interactions to investigate possible exotic states. The predicted molecular state is consistent with the latest finding T_{cc} [3]. In the present work, we extend it to investigate the charmed-anticharmed system $D\bar{D}^*$. As we mentioned in Sec. I, various XYZ states were observed around open-charm thresholds, therefore the elaborate heavy-meson interactions studied here may help us to reveal the natures and inner structures of these charmoniumlike states.

The generalization of the previous work is not straightforward. In this work, we first construct $D\bar{D}^*$ interacting Lagrangians by properly considering the charge conjugation properties of the fields in the heavy quark limit. We then calculate S-wave $D\bar{D}^*$ potentials up to $O(\epsilon^2)$ order at one-loop level using Weinberg's scheme. Complete contact, OPE and TPE interactions are included. For a deeper understanding of the $D\bar{D}^*$ interactions, we further solve the Schrödinger equations to find the bound state solutions using the calculated potentials.

Behaviors of the $D\bar{D}^*$ potentials as well as bound state properties are analyzed in detail. In considered four channels, i.e., $I^G(J^{PC}) = 0^+(1^{++})$, $0^-(1^{+-})$, $1^-(1^{++})$, and $1^+(1^{+-})$, distinct behaviors appear depending on the competitions of the contribution carrying contact interactions, OPE and TPE contributions. This leads to a specific mechanism of the bound state formation in each channel. For example, in the $0^+(1^{++})$ and $0^-(1^{+-})$ channels, relatively large repulsions of the TPE contributions cause them to have weak bindings.

Combining the potential behaviors and the bound state properties, we conclude that there exists a strength ordering of the $D\bar{D}^*$ interactions in the four channels that would lead to different binding abilities:

$$\text{str.}[0^+(1^{++})] > \text{str.}[0^-(1^{+-})] > \text{str.}[1^+(1^{+-})]$$
$$> \text{str.}[1^-(1^{++})], \tag{58}$$

where str. stands for the strength of the interaction.

Further, our investigation reveals that the $D\bar{D}^*$ interaction in the $0^+(1^{++})$ channel is strongly responsible for experimentally discovered $X(3872)$, so $X(3872)$ can be a good candidate of the $0^+(1^{++})$ molecular state. In addition, $D\bar{D}^*$ also tends to form molecular states in the $0^-(1^{+-})$ and $1^+(1^{+-})$ channels.

We also examine the potential behaviors of the $0^-(1^{+-})$ and $1^+(1^{+-})$ molecular states in detail, and point out their formation mechanisms. Their discovery potentials are also discussed. We hope future experiments such as BESIII, LHCb, and Belle II can further study them in the e^+e^- productions and b decays, to search for the predicted multiple structures around the $D\bar{D}^*$ mass region. Besides, we also expect that they can be searched in future $\bar{P}$ANDA experiment.

APPENDIX: DETERMINATION OF THE UNKNOWN LECS

Assuming contact contributions from Eq. (7) are equivalent to the ρ, ω, and σ exchanges, we will be able to extract D_a, D_b, E_a, and E_b.

For the ρ, ω, and σ exchanges, we need corresponding interacting Lagrangians for the $D^{(*)}D^{(*)}V$ and $D^{(*)}D^{(*)}\sigma$ vertexes:

$$\mathcal{L}_{HV} = i\beta\langle Hv_\mu(-V^\mu)\bar{H}\rangle + i\lambda\langle H\sigma_{\mu\nu}F^{\mu\nu}(\rho)\bar{H}\rangle, \quad (A1)$$

$$\mathcal{L}_{H\sigma} = g_s\langle H\sigma\bar{H}\rangle, \quad (A2)$$

as well as their charge conjugations:

$$\mathcal{L}_{HcV} = -i\beta\langle \bar{H}_c v_\mu(-V^\mu)H_c\rangle + i\lambda\langle \bar{H}_c\sigma_{\mu\nu}F^{\mu\nu}(V)H_c\rangle, \quad (A3)$$

$$\mathcal{L}_{Hc\sigma} = g_s\langle \bar{H}_c\sigma H_c\rangle, \quad (A4)$$

where $F_{\mu\nu}(V) = \partial_\mu V_\nu - \partial_\nu V_\mu + [V_\mu, V_\nu]$ and

$$V = \frac{ig_V}{\sqrt{2}}\begin{pmatrix} \frac{\rho^0}{\sqrt{2}} + \frac{\omega}{\sqrt{2}} & \rho^+ \\ \rho^- & -\frac{\rho^0}{\sqrt{2}} + \frac{\omega}{\sqrt{2}} \end{pmatrix}. \quad (A5)$$

In above, H and H_c has been defined in Eqs. (2) and (6), $g_V = 5.8$, $\beta = 0.9$, $\lambda = 0.56$ GeV^{-1} [96], $g_s = \frac{3.73}{2\sqrt{6}}$ [97].

By matching the $D\bar{D}^* \to D\bar{D}^*$ amplitudes in the two ways, we get

$$D_a \sim -\frac{g_s^2}{m_\sigma^2} - \frac{\beta^2 g_v^2}{4m_\omega^2}, \qquad E_a \sim -\frac{\beta^2 g_v^2}{4m_\rho^2},$$

$$D_b \sim 0, \qquad E_b \sim 0. \quad (A6)$$

[1] R. Aaij *et al.* (LHCb Collaboration), Observation of structure in the J/ψ -pair mass spectrum, Sci. Bull. **65,** 1983 (2020).

[2] R. Aaij *et al.* (LHCb Collaboration), Amplitude analysis of the $B^+ \to D^+D^-K^+$ decay, Phys. Rev. D **102,** 112003 (2020).

[3] R. Aaij *et al.* (LHCb Collaboration), Observation of an exotic narrow doubly charmed tetraquark, arXiv:2109.01038.

[4] H. X. Chen, W. Chen, X. Liu, and S. L. Zhu, The hidden-charm pentaquark and tetraquark states, Phys. Rep. **639,** 1 (2016).

[5] A. Esposito, A. Pilloni, and A. D. Polosa, Multiquark resonances, Phys. Rep. **668,** 1 (2017).

[6] R. F. Lebed, R. E. Mitchell, and E. S. Swanson, Heavy-quark QCD exotica, Prog. Part. Nucl. Phys. **93,** 143 (2017).

[7] F. K. Guo, C. Hanhart, and U. G. Meißner, Q. Wang, Q. Zhao, and B. S. Zou, Hadronic molecules, Rev. Mod. Phys. **90,** 015004 (2018).

[8] Y. R. Liu, H. X. Chen, W. Chen, X. Liu, and S. L. Zhu, Pentaquark and Tetraquark states, Prog. Part. Nucl. Phys. **107,** 237 (2019).

[9] N. Brambilla, S. Eidelman, C. Hanhart, A. Nefediev, C. P. Shen, C. E. Thomas, A. Vairo, and C. Z. Yuan, The *XYZ* states: Experimental and theoretical status and perspectives, Phys. Rep. **873,** 1 (2020).

[10] S. K. Choi *et al.* (Belle Collaboration), Observation of a Narrow Charmonium-Like State in Exclusive $B^{+(-)} \to K^{+(-)}\pi^+\pi^-J/\psi$ Decays, Phys. Rev. Lett. **91,** 262001 (2003).

[11] S. Godfrey and N. Isgur, Mesons in a relativized quark model with chromodynamics, Phys. Rev. D **32,** 189 (1985).

[12] M. Ablikim *et al.* (BESIII Collaboration), Observation of a Charged Charmoniumlike Structure in $e^+e^- \to \pi^+\pi^-J/\psi$ at $\sqrt{s} = 4.26$ GeV, Phys. Rev. Lett. **110,** 252001 (2013).

[13] Z. Q. Liu *et al.* (Belle Collaboration), Study of $e^+e^- \to \pi^+\pi^-J/\psi$ and Observation of a Charged Charmonium-like State at Belle, Phys. Rev. Lett. **110,** 252002 (2013); Erratum, Phys. Rev. Lett. **111,** 019901 (2013).

[14] M. Ablikim *et al.* (BESIII Collaboration), Observation of a Charged Charmoniumlike Structure $Z_c(4020)$ and Search for the $Z_c(3900)$ in $e^+e^- \to \pi^+\pi^-h_c$, Phys. Rev. Lett. **111,** 242001 (2013).

[15] K. Abe *et al.* (Belle Collaboration), Observation of a Near-Threshold Omega J/ψ Mass Enhancement in Exclusive $B \to K\omega J/\psi$ Decays, Phys. Rev. Lett. **94,** 182002 (2005).

[16] T. Aaltonen *et al.* (CDF Collaboration), Evidence for a Narrow Near-Threshold Structure in the $J/\psi\phi$ Mass Spectrum in $B^+ \rightarrow J/\psi\phi K^+$ Decays, Phys. Rev. Lett. **102,** 242002 (2009).

[17] S. K. Choi *et al.* (Belle Collaboration), Observation of a Resonance-Like Structure in the $pi^{\pm}\psi'$ Mass Distribution in Exclusive $B \rightarrow K\pi^{\pm}\psi'$ Decays, Phys. Rev. Lett. **100,** 142001 (2008).

[18] S. Jia *et al.* (Belle Collaboration), Observation of a vector charmoniumlike state in $e^+e^- \rightarrow D_s^+ D_{s1}(2536)^- + $ c.c., Phys. Rev. D **100,** 111103 (2019).

[19] S. Jia *et al.* (Belle Collaboration), Evidence for a vector charmoniumlike state in $e^+e^- \rightarrow D_s^+ D_{s2}^*(2573)^- + $ c.c., Phys. Rev. D **101,** 091101 (2020).

[20] F. L. Wang, X. D. Yang, R. Chen, and X. Liu, Correlation of the hidden-charm molecular tetraquarks and the charmoniumlike structures existing in the $B \rightarrow XYZ + K$ process, Phys. Rev. D **104,** 094010 (2021).

[21] S. Weinberg, Nuclear forces from chiral Lagrangians, Phys. Lett. B **251,** 288 (1990).

[22] S. Weinberg, Effective chiral Lagrangians for nucleon—pion interactions and nuclear forces, Nucl. Phys. **B363,** 3 (1991).

[23] C. Ordonez and U. van Kolck, Chiral lagrangians and nuclear forces, Phys. Lett. B **291,** 459 (1992).

[24] C. Ordonez, L. Ray, and U. van Kolck, The two nucleon potential from chiral Lagrangians, Phys. Rev. C **53,** 2086 (1996).

[25] E. Epelbaum, W. Gloeckle, and U. G. Meissner, Nuclear forces from chiral Lagrangians using the method of unitary transformation. 1. Formalism, Nucl. Phys. **A637,** 107 (1998).

[26] E. Epelbaum, W. Gloeckle, and U. G. Meissner, Nuclear forces from chiral Lagrangians using the method of unitary transformation. 2. The two nucleon system, Nucl. Phys. **A671,** 295 (2000).

[27] M. P. Valderrama, Perturbative renormalizability of chiral two pion exchange in nucleon-nucleon scattering, Phys. Rev. C **83,** 024003 (2011).

[28] M. Pavon Valderrama, Perturbative renormalizability of chiral two pion exchange in nucleon-nucleon scattering: P- and D-waves, Phys. Rev. C **84,** 064002 (2011).

[29] B. Long and C. J. Yang, Renormalizing chiral nuclear forces: A case study of $^3P_0$, Phys. Rev. C **84,** 057001 (2011).

[30] B. Long and C. J. Yang, Short-range nuclear forces in singlet channels, Phys. Rev. C **86,** 024001 (2012).

[31] X. W. Kang, J. Haidenbauer, and U. G. Meissner, Antinucleon-nucleon interaction in chiral effective field theory, J. High Energy Phys. 02 (**2014**) 113.

[32] E. Epelbaum, H. Krebs, and U. G. Meissner, Improved chiral nucleon-nucleon potential up to next-to-next-to-next-to-leading order, Eur. Phys. J. A **51,** 53 (2015).

[33] B. Long and Y. Mei, Cutoff regulators in chiral nuclear effective field theory, Phys. Rev. C **93,** 044003 (2016).

[34] L. Y. Dai, J. Haidenbauer, and U. G. Meissner, Antinucleon-nucleon interaction at next-to-next-to-next-to-leading order in chiral effective field theory, J. High Energy Phys. 07 (2017) 078.

[35] K. W. Li, T. Hyodo, and L. S. Geng, Strangeness $S = -2$ baryon-baryon interactions in relativistic chiral effective field theory, Phys. Rev. C **98,** 065203 (2018).

[36] X. L. Ren, K. W. Li, L. S. Geng, B. W. Long, P. Ring, and J. Meng, Leading order relativistic chiral nucleon-nucleon interaction, Chin. Phys. C **42,** 014103 (2018).

[37] Y. Xiao, L. S. Geng, and X. L. Ren, Covariant chiral nucleon-nucleon contact Lagrangian up to order $\mathcal{O}(q^4)$, Phys. Rev. C **99,** 024004 (2019).

[38] S. Wu and B. Long, Perturbative NN scattering in chiral effective field theory, Phys. Rev. C **99,** 024003 (2019).

[39] V. Baru, E. Epelbaum, J. Gegelia, and X. L. Ren, Towards baryon-baryon scattering in manifestly Lorentz-invariant formulation of SU(3) baryon chiral perturbation theory, Phys. Lett. B **798,** 134987 (2019).

[40] X. L. Ren, E. Epelbaum, and J. Gegelia, Λ-nucleon scattering in baryon chiral perturbation theory, Phys. Rev. C **101,** 034001 (2020).

[41] Z. Liu, L. H. Wen, and J. F. Yang, Covariant propagator and chiral power counting, Nucl. Phys. **B963,** 115288 (2021).

[42] Q. Q. Bai, C. X. Wang, Y. Xiao, and L. S. Geng, Pion-mass dependence of the nucleon-nucleon interaction, Phys. Lett. B **809,** 135745 (2020).

[43] Y. Xiao, C. X. Wang, J. X. Lu, and L. S. Geng, Two-pion exchange contributions to the nucleon-nucleon interaction in covariant baryon chiral perturbation theory, Phys. Rev. C **102,** 054001 (2020).

[44] C. X. Wang, L. S. Geng, and B. Long, Renormalizability of leading order covariant chiral nucleon-nucleon interaction, Chin. Phys. C **45,** 054101 (2021).

[45] E. Epelbaum, H. W. Hammer, and U. G. Meissner, Modern theory of nuclear forces, Rev. Mod. Phys. **81,** 1773 (2009).

[46] R. Machleidt and D. R. Entem, Chiral effective field theory and nuclear forces, Phys. Rep. **503,** 1 (2011).

[47] R. Machleidt and F. Sammarruca, Chiral EFT based nuclear forces: Achievements and challenges, Phys. Scr. **91,** 083007 (2016).

[48] U. G. Meissner, The long and winding road from chiral effective Lagrangians to nuclear structure, Phys. Scr. **91,** 033005 (2016).

[49] E. Epelbaum, H. Krebs, and P. Reinert, High-precision nuclear forces from chiral EFT: State-of-the-art, challenges and outlook, Front. Phys. **8,** 98 (2020).

[50] Z. W. Liu, N. Li, and S. L. Zhu, Chiral perturbation theory and the $\bar{B}B$ strong interaction, Phys. Rev. D **89,** 074015 (2014).

[51] H. Xu, B. Wang, Z. W. Liu, and X. Liu, DD^* potentials in chiral perturbation theory and possible molecular states, Phys. Rev. D **99,** 014027 (2019).

[52] B. Wang, Z. W. Liu, and X. Liu, $\bar{B}^{(*)}\bar{B}^{(*)}$ interactions in chiral effective field theory, Phys. Rev. D **99,** 036007 (2019).

[53] L. Meng, B. Wang, G. J. Wang, and S. L. Zhu, The hidden charm pentaquark states and $\Sigma_c\bar{D}^{(*)}$ interaction in chiral perturbation theory, Phys. Rev. D **100,** 014031 (2019).

[54] B. Wang, L. Meng, and S. L. Zhu, Spectrum of the strange hidden charm molecular pentaquarks in chiral effective field theory, Phys. Rev. D **101,** 034018 (2020).

[55] B. Wang, L. Meng, and S. L. Zhu, Hidden-charm and hidden-bottom molecular pentaquarks in chiral effective field theory, J. High Energy Phys. 11 (2019) 108.

[56] L. Meng, B. Wang, and S. L. Zhu, $\Sigma_c N$ interaction in chiral effective field theory, Phys. Rev. C **101,** 064002 (2020).

[57] B. Wang, L. Meng, and S. L. Zhu, $D^{(*)}N$ interaction and the structure of $\Sigma_c(2800)$ and $\Lambda_c(2940)$ in chiral effective field theory, Phys. Rev. D **101,** 094035 (2020).

[58] K. Chen, B. Wang, and S. L. Zhu, Exploration of the doubly charmed molecular pentaquarks, Phys. Rev. D **103,** 116017 (2021).

[59] Y. R. Liu, X. Liu, W. Z. Deng, and S. L. Zhu, Is $X(3872)$ really a molecular state?, Eur. Phys. J. C **56,** 63 (2008).

[60] X. Liu, Z. G. Luo, Y. R. Liu, and S. L. Zhu, X(3872) and other possible heavy molecular states, Eur. Phys. J. C **61,** 411 (2009).

[61] N. Li and S. L. Zhu, Isospin breaking, coupled-channel effects and diagnosis of X(3872), Phys. Rev. D **86,** 074022 (2012).

[62] L. Zhao, L. Ma, and S. L. Zhu, Spin-orbit force, recoil corrections, and possible $B\bar{B}^*$ and $D\bar{D}^*$ molecular states, Phys. Rev. D **89,** 094026 (2014).

[63] M. Z. Liu, T. W. Wu, M. Pavon Valderrama, J. J. Xie, and L. S. Geng, Heavy-quark spin and flavor symmetry partners of the X(3872) revisited: What can we learn from the one boson exchange model?, Phys. Rev. D **99,** 094018 (2019).

[64] M. T. AlFiky, F. Gabbiani, and A. A. Petrov, X(3872): Hadronic molecules in effective field theory, Phys. Lett. B **640,** 238 (2006).

[65] A. De Rujula, H. Georgi, and S. L. Glashow, Molecular Charmonium: A New Spectroscopy?, Phys. Rev. Lett. **38,** 317 (1977).

[66] N. A. Tornqvist, From the deuteron to deusons, an analysis of deuteronlike meson-meson bound states, Z. Phys. C **61,** 525 (1994).

[67] C. Y. Wong, Molecular states of heavy quark mesons, Phys. Rev. C **69,** 055202 (2004).

[68] E. S. Swanson, Short range structure in the X(3872), Phys. Lett. B **588,** 189 (2004).

[69] M. B. Voloshin, Interference and binding effects in decays of possible molecular component of X(3872), Phys. Lett. B **579,** 316 (2004).

[70] F. E. Close and P. R. Page, The $D^{*0}\bar{D}^0$ threshold resonance, Phys. Lett. B **578,** 119 (2004).

[71] N. A. Tornqvist, Isospin breaking of the narrow charmonium state of Belle at 3872 MeV as a deuson, Phys. Lett. B **590,** 209 (2004).

[72] M. Suzuki, The X(3872) boson: Molecule or charmonium, Phys. Rev. D **72,** 114013 (2005).

[73] Y. J. Zhang, H. C. Chiang, P. N. Shen, and B. S. Zou, Possible S-wave bound-states of two pseudoscalar mesons, Phys. Rev. D **74,** 014013 (2006).

[74] C. E. Thomas and F. E. Close, Is X(3872) a molecule?, Phys. Rev. D **78,** 034007 (2008).

[75] I. W. Lee, A. Faessler, T. Gutsche, and V. E. Lyubovitskij, X(3872) as a molecular DD^* state in a potential model, Phys. Rev. D **80,** 094005 (2009).

[76] G. J. Ding, J. F. Liu, and M. L. Yan, Dynamics of hadronic molecule in one-boson exchange approach and possible heavy flavor molecules, Phys. Rev. D **79,** 054005 (2009).

[77] Z. F. Sun, J. He, X. Liu, Z. G. Luo, and S. L. Zhu, $Z_b(10610)^\pm$ and $Z_b(10650)^\pm$ as the $B^*\bar{B}$ and $B^*\bar{B}^*$ molecular states, Phys. Rev. D **84,** 054002 (2011).

[78] Z. F. Sun, Z. G. Luo, J. He, X. Liu, and S. L. Zhu, A note on the $B^*\bar{B}$, $B^*\bar{B}^*$, $D^*\bar{D}$, $D^*\bar{D}^*$, molecular states, Chin. Phys. C **36,** 194 (2012).

[79] J. He, Study of the $B\bar{B}^*/D\bar{D}^*$ bound states in a Bethe-Salpeter approach, Phys. Rev. D **90,** 076008 (2014).

[80] Y. C. Yang, Z. Y. Tan, J. Ping, and H. S. Zong, Possible $D^{(*)}\bar{D}^{(*)}$ and $B^{(*)}\bar{B}^{(*)}$ molecular states in the extended constituent quark models, Eur. Phys. J. C **77,** 575 (2017).

[81] Z. Y. Wang, J. J. Qi, X. H. Guo, and C. Wang, X(3872) as a molecular $D\bar{D}^*$ state in the Bethe-Salpeter equation approach, Phys. Rev. D **97,** 016015 (2018).

[82] B. X. Sun, D. M. Wan, and S. Y. Zhao, The $D\bar{D}^*$ interaction with isospin zero in an extended hidden gauge symmetry approach, Chin. Phys. C **42,** 053105 (2018).

[83] Z. M. Ding, H. Y. Jiang, and J. He, Molecular states from $D^{(*)}\bar{D}^{(*)}/B^{(*)}\bar{B}^{(*)}$ and $D^{(*)}D^{(*)}/\bar{B}^{(*)}\bar{B}^{(*)}$ interactions, Eur. Phys. J. C **80,** 1179 (2020).

[84] M. J. Zhao, Z. Y. Wang, C. Wang, and X. H. Guo, Investigation of the possible $D\bar{D}^*/B\bar{B}^*$ and $DD^*/\bar{B}\bar{B}^*$ molecule states, arXiv:2112.12633.

[85] G. Burdman and J. F. Donoghue, Union of chiral and heavy quark symmetries, Phys. Lett. B **280,** 287 (1992).

[86] M. B. Wise, Chiral perturbation theory for hadrons containing a heavy quark, Phys. Rev. D **45,** R2188 (1992).

[87] T. M. Yan, H. Y. Cheng, C. Y. Cheung, G. L. Lin, Y. C. Lin, and H. L. Yu, Heavy quark symmetry and chiral dynamics, Phys. Rev. D **46,** 1148 (1992); Erratum, Phys. Rev. D **55,** 5851 (1997).

[88] M. Ablikim et al. (BESIII Collaboration), Observation of $Z_c(3900)^0$ in $e^+e^- \to \pi^0\pi^0 J/\psi$, Phys. Rev. Lett. **115,** 112003 (2015).

[89] V. M. Abazov et al. (D0 Collaboration), Evidence for $Z_c^\pm(3900)$ in semi-inclusive decays of b-flavored hadrons, Phys. Rev. D **98,** 052010 (2018).

[90] K. Chilikin et al. (Belle Collaboration), Observation of a new charged charmoniumlike state in $\bar{B}^0 \to J/\psi K^-\pi^+$ decays, Phys. Rev. D **90,** 112009 (2014).

[91] R. Aaij et al. (LHCb Collaboration), Model-Independent Observation of Exotic Contributions to $B^0 \to J/\psi K^+\pi^-$ Decays, Phys. Rev. Lett. **122,** 152002 (2019).

[92] B. Aubert et al. (BABAR Collaboration), Observation of the Decay $B \to J/\psi\eta K$ and Search for $X(3872) \to J/\psi\eta$, Phys. Rev. Lett. **93,** 041801 (2004).

[93] T. Iwashita et al. (Belle Collaboration), Measurement of branching fractions for $B \to J/\psi\eta K$ decays and search for a narrow resonance in the $J/\psi\eta$ final state, Prog. Theor. Exp. Phys. **2014,** 043C01 (2014).

[94] A. Vinokurova et al. (Belle Collaboration), Search for B decays to final states with the η_c meson, J. High Energy Phys. 06 (2015) 132; Erratum, J. High Energy Phys. 02 (2017) 88.

[95] J. P. Lees et al. (BABAR Collaboration), Measurements of the Absolute Branching Fractions of $B^\pm \to K^\pm X_{c\bar{c}}$, Phys. Rev. Lett. **124,** 152001 (2020).

[96] N. Li, Z. F. Sun, X. Liu, and S. L. Zhu, Coupled-channel analysis of the possible $D^{(*)}D^{(*)}$, $\bar{B}^{(*)}\bar{B}^{(*)}$ and $D^{(*)}\bar{B}^{(*)}$ molecular states, Phys. Rev. D **88,** 114008 (2013).

[97] W. A. Bardeen, E. J. Eichten, and C. T. Hill, Chiral multiplets of heavy—light mesons, Phys. Rev. D **68,** 054024 (2003).